New Trends on Magnetic Sensors

Pilar Marín

INSTITUTO DE MAGNETISMO APLICADO
LABORATORIO SALVADOR VELAYOS UCM ADIF

ESMoINa 2024

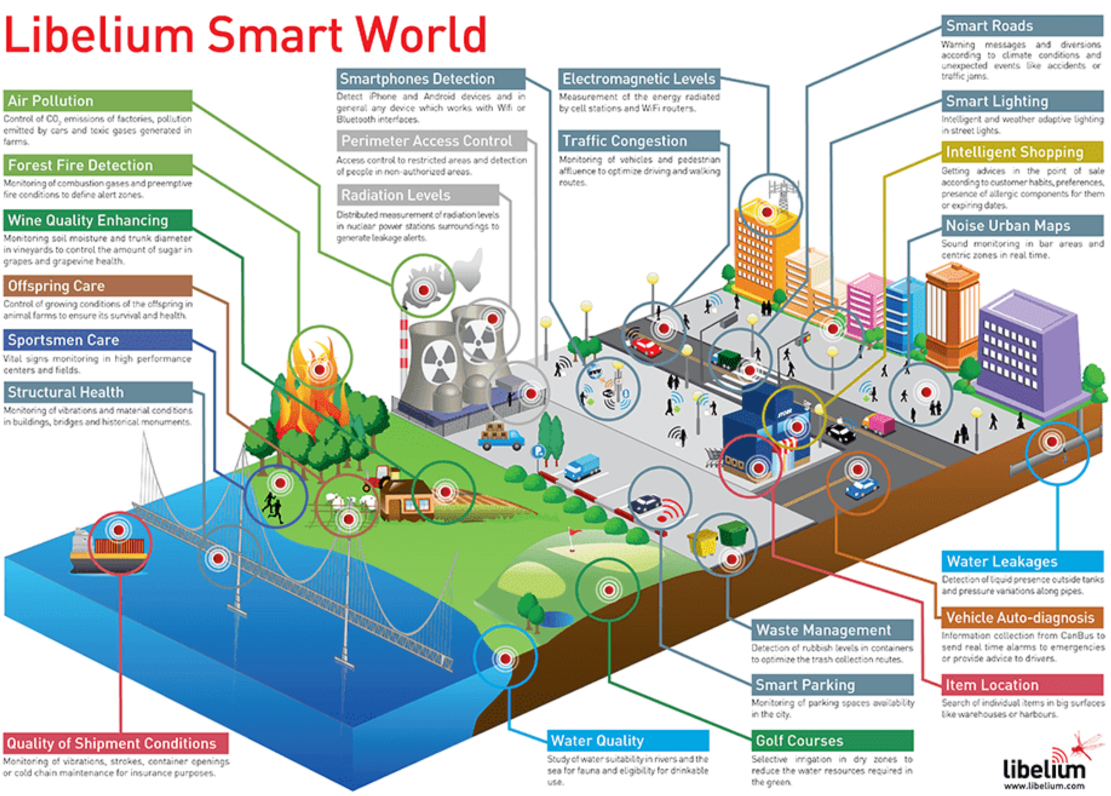

IEEE TRANSACTIONS ON MAGNETICS 1

Advances in Magnetics

Overview of Spintronic Sensors With Internet of Things for Smart Living

Xuyang Liu[1], K. H. Lam[1], Ke Zhu[1], Chao Zheng[1], Xu Li[1], Yimeng Du[1], Chunhua Liu[2], and Philip W. T. Pong[1]

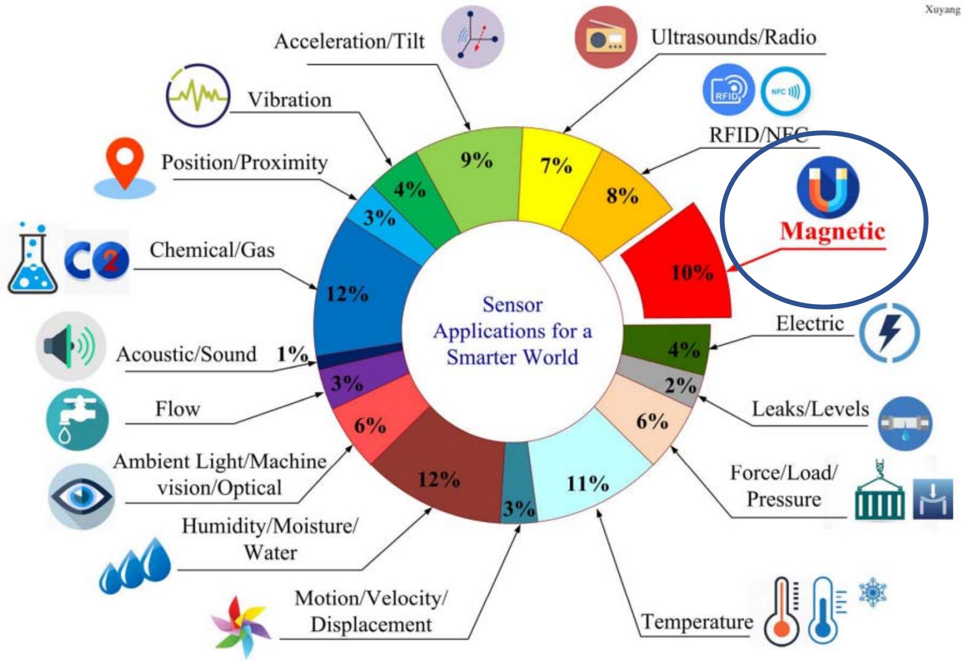

Chemiresistive sensors

Response = $\Delta R/R_0 = (R - R_0)/R_0$,

Sensors & Actuators: B. Chemical 335 (2021) 129657

Contents lists available at ScienceDirect

Sensors and Actuators: B. Chemical

journal homepage: www.elsevier.com/locate/snb

Ultrasensitive NO_2 gas sensor with insignificant NH_3-interference based on a few-layered mesoporous graphene

Daniel Matatagui, Jesús López-Sánchez, Alvaro Peña, Aída Serrano, Adolfo del Campo, Oscar Rodríguez de la Fuente, Noemí Carmona, Elena Navarro, ... Carmen Horrillo

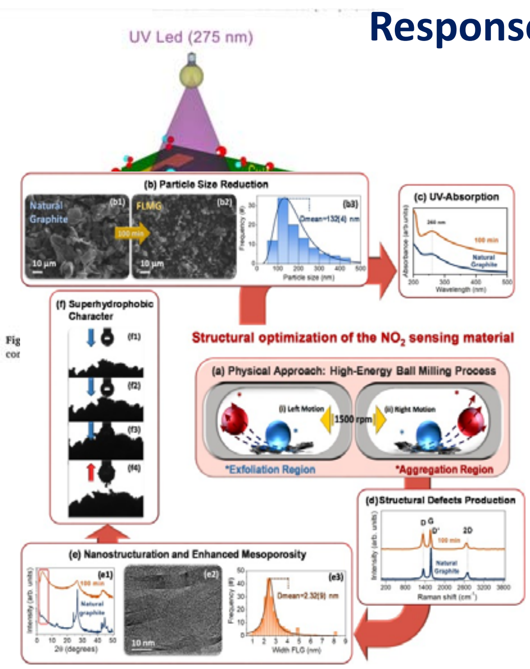

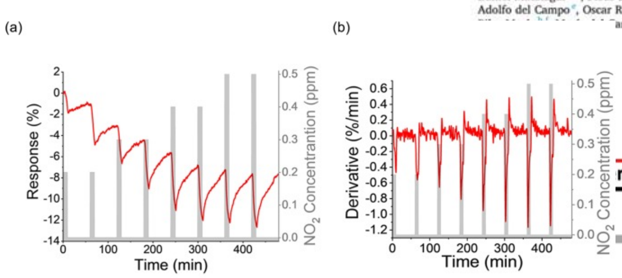

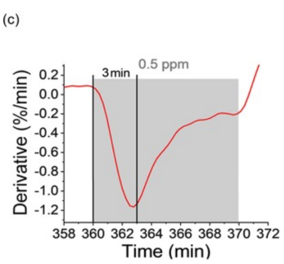

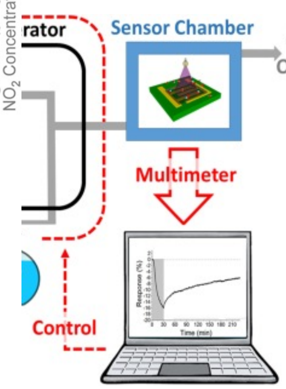

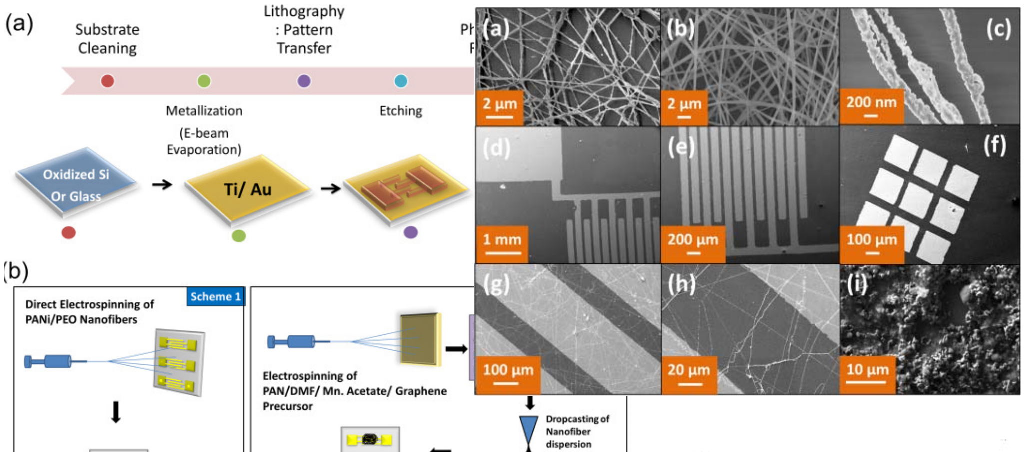

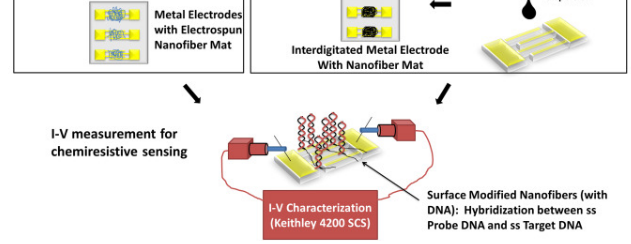

Biosensors and Bioelectronics
Volume 133, 15 May 2019, Pages 24-31

Chemiresistive DNA hybridization sensor with electrospun nanofibers: A method to minimize inter-device variability

Suryasnata Tripathy [a], Vasundhra Bhandari [b], Paresh Sharma [b], Siva Rama Krishna Vanjari [a], Shiv Govind Singh [a]

DNAs corresponding to Staphylococcus aureus specific genes, namely nuc, mecA, vanA and protein A.

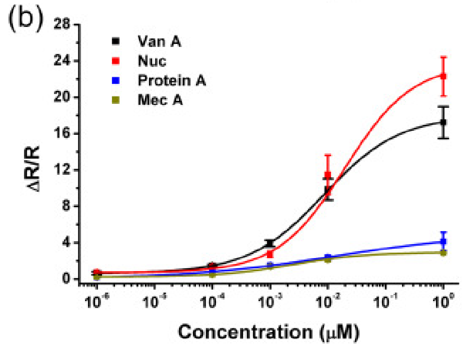

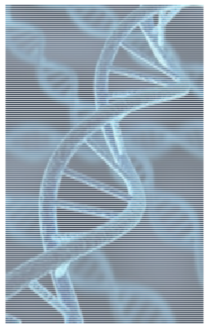

Surface Acoustic Waves sensors

View PDF
Download full issue
Sensors and Actuators B: Chemical
Volume 154, Issue 2, 20 June 2011, Pages 199-205

Chemical warfare agents simulants ... nized SAW sensor

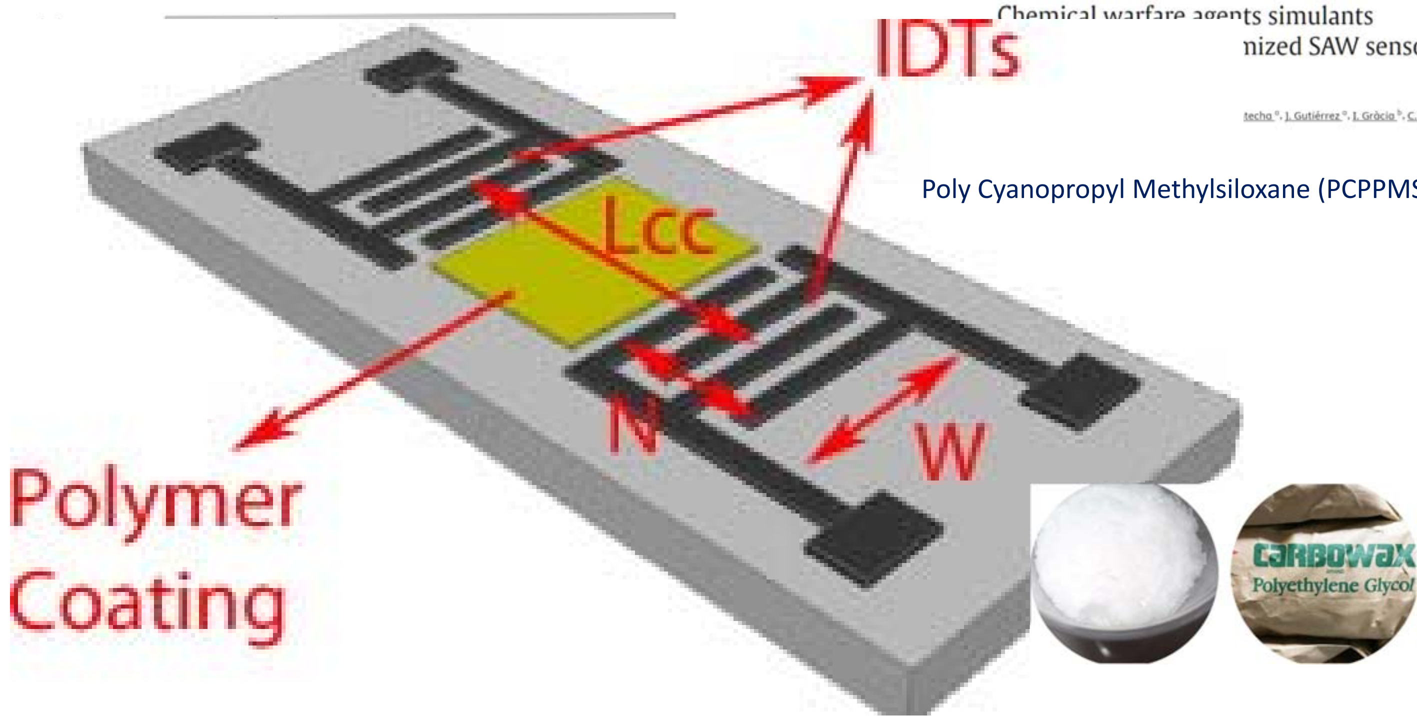

Poly Cyanopropyl Methylsiloxane (PCPPMS)

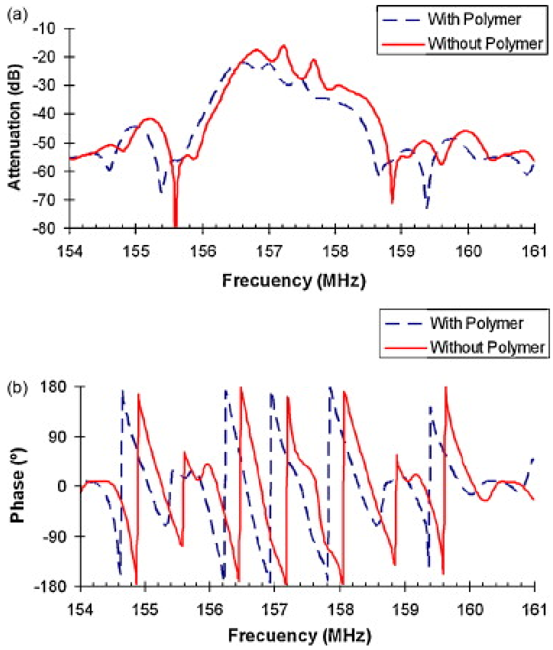

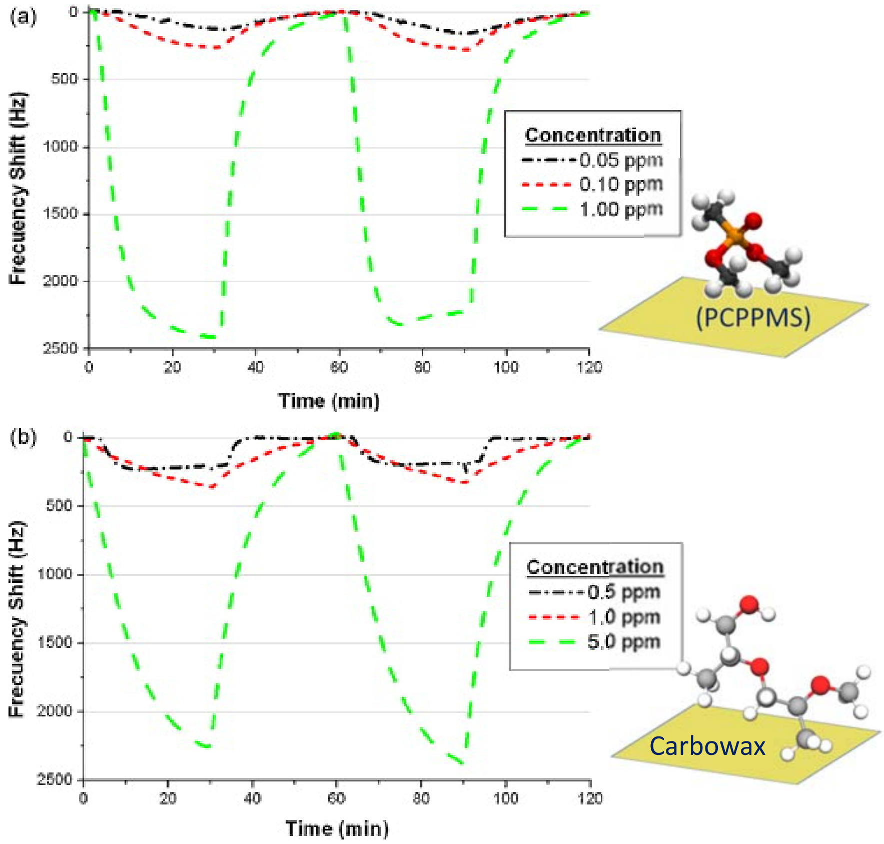

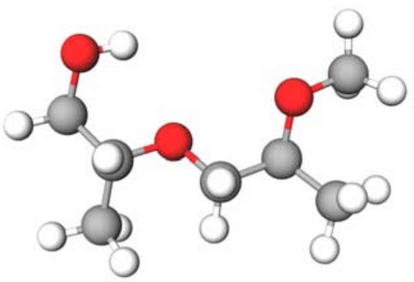

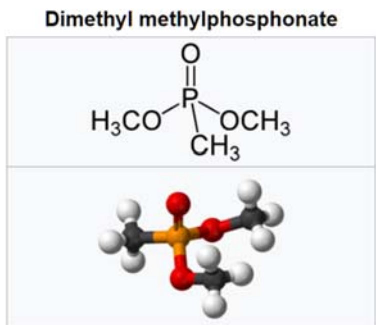

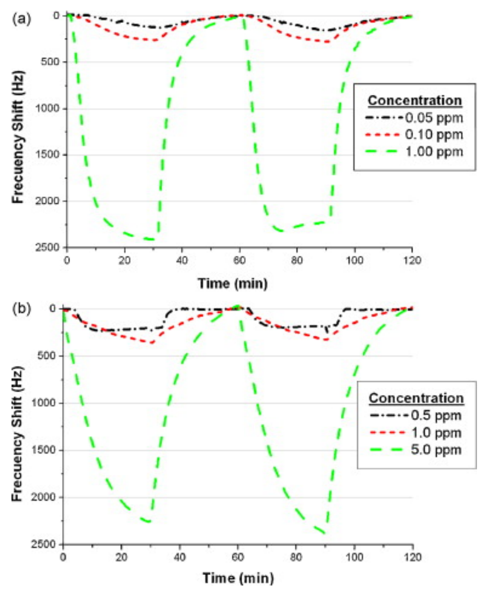

dipropylene
glycol monomethyl ether (DPGME).

Polycyanopropylmethylsiloxane (PCPMS)

Fig. 6. Response curves for very low concentrations. (a) DMMP and sensor coated with PCPMS and(b) DPGMEandsensor coated with Carbowax.

Micromechanical resonators: cantilever

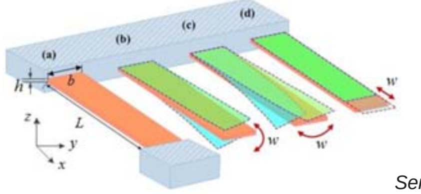

Sensors **2015**, *15*(10), 26478-26566

Figure 1. Schematic diagram of the beam-based resonators. Doubly clamped beam (**a**) and cantilever beam with the flexural (out-of-plane) mode (**b**), the lateral (in-plane) bending mode (**c**) and the elongation (in-plane) mode (**d**).

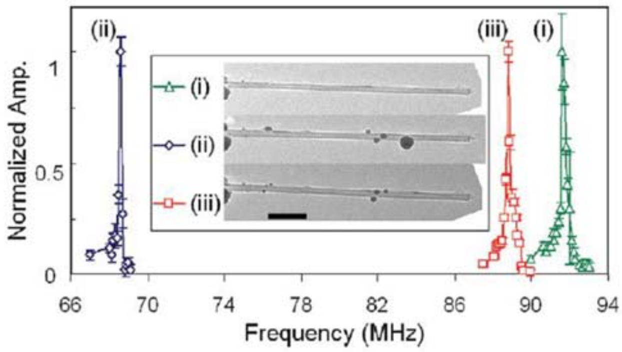

Figure 8. Resonant frequency shifts in MWNT nanomechanical resonators due to mass migration. Reused with permission from [97], Copyright 2009, American Chemical Society.

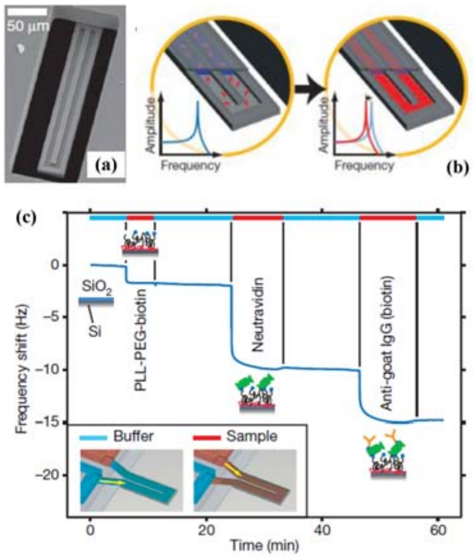

Figure 12. A suspended microchannel microresonator for biomolecular mass sensing reported by Burg *et al*. [163]. Reused with permission from [163], Copyright 2007 Nature Publishing Group. (**a**) Schematic of mass measurement mode by a microcantilever; (**b**) Resonant frequency shifts caused by accumulation of proteins inside the cantilever.

THE JOURNAL OF PHYSICAL CHEMISTRY C

Article

Cite This: J. Phys. Chem. C 2019, 123, 6778−6786

pubs.acs.org/JPCC

Sensing of the Molecular Spin in Spin-Crossover Nanoparticles with Micromechanical Resonators

Julien Dugay,[*,†] Mónica Giménez-Marqués,[‡] Warner J. Venstra,[†] Ramón Torres-Cavanillas,[‡] Umit N. Sheombarsing,[†] Nicola Manca,[†,§] Eugenio Coronado,[*,‡] and Herre S. J. van der Zant[†]

Fe_{II}-based spin-crossover nanoparticles of the well-known

[Fe(Htrz)2(trz)](BF4)

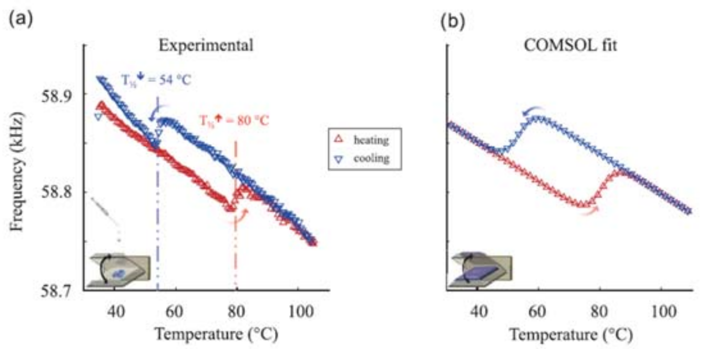

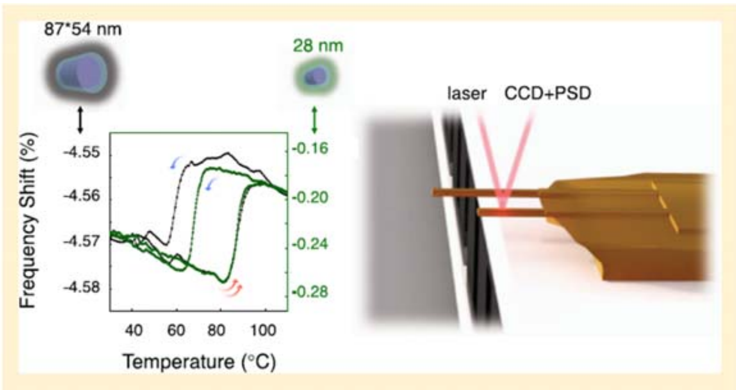

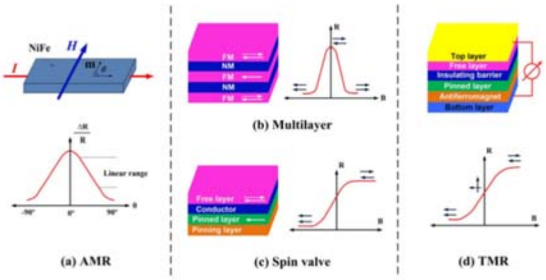

Spintronic

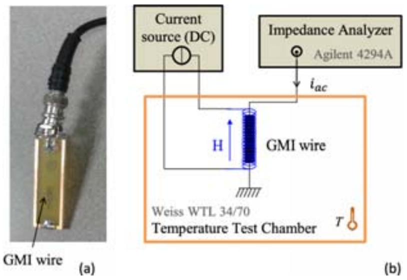

Giant Magnetoimpedance

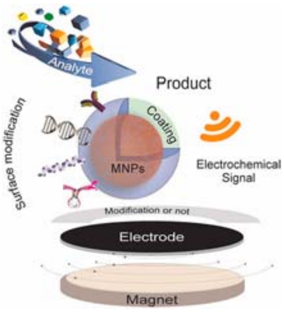

Magnetic

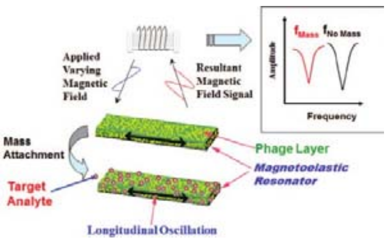

Magnetoelasticity

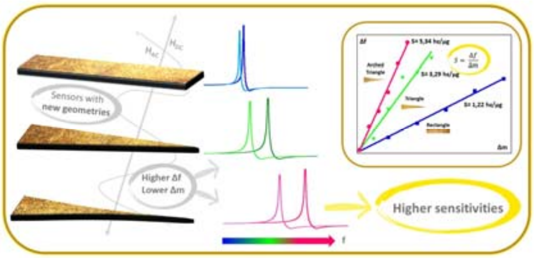

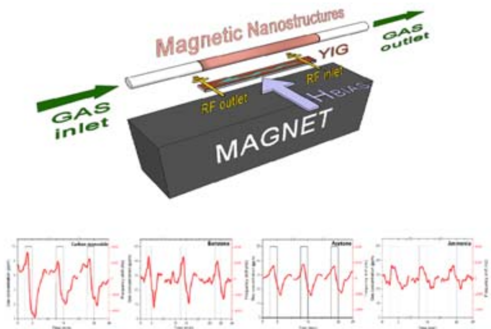

Spin waves

Magnetic Transducers

Magnetoelasticity

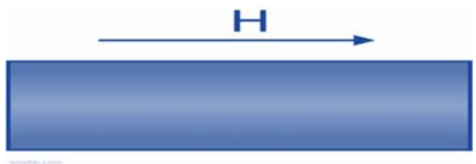

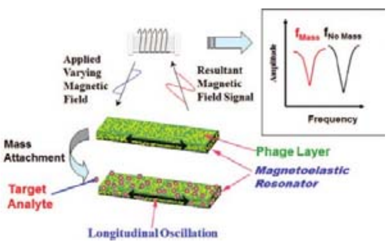

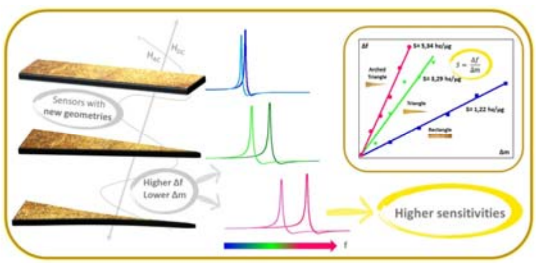

SENSOR PRINCIPLE

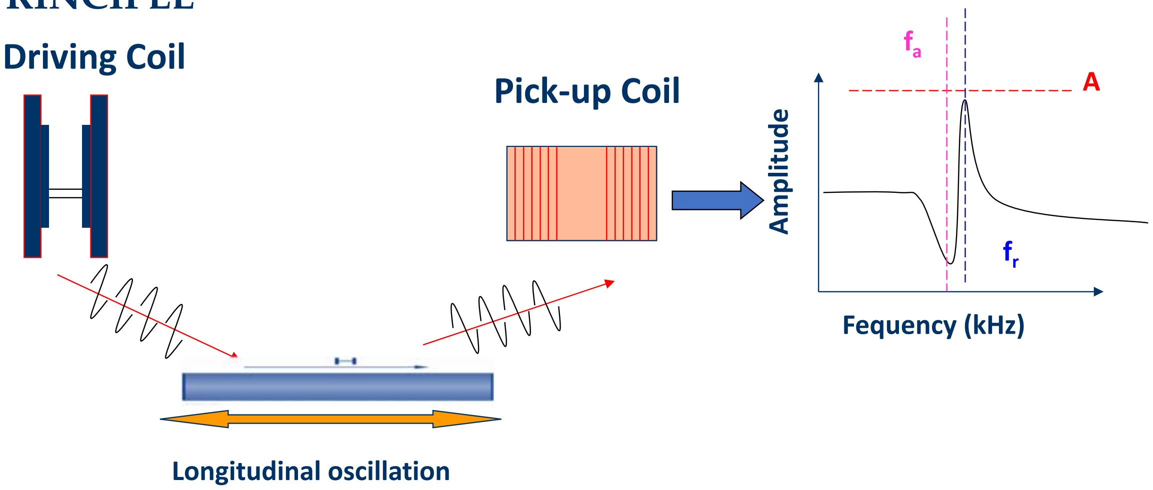

Measurements of the resonance frequency are performed by using a magnetoelastic resonance analyzer set up.

The variation in the pick-up coil impedance with frequency allows the observation of resonance,f_r, and antiresonance,f_a, frequencies of the microwire.

Magnetoelastic resonance-based gas sensors

We excite the magnetoelastic with an **alternating magnetic field** in a **frequency sweep** and we see the changes in its magnetization with a pick-up coil.

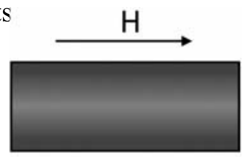

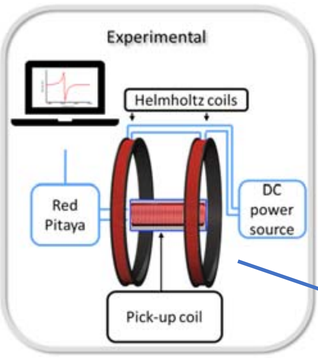

$$f_0 = \frac{1}{2L}\sqrt{\frac{E_H}{\rho(1-\upsilon)}}$$

Changes in the deposited mass over the sensor will change its resonant frequency:

$$f = f_0\sqrt{\frac{1}{1+\frac{\Delta m}{m_0}}} \rightarrow \frac{\Delta f}{f_0} = -\frac{\Delta m}{2m_0}$$

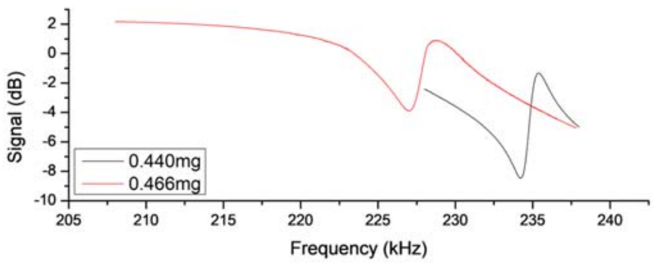

Motivation:
Contactless low-cost sensors (various applications)

ELASTIC WAVE EQUATION

Longitudinal vibration (y direction)

u: Displacement
ρ: Density
E: Young´s modulus
ν: Poisson ration
l: Length of the wire

$$\frac{\rho\left(1-\sigma^2\right)}{E}\frac{\delta^2 u}{\delta^2 t}+\frac{\delta u}{\delta t}=\frac{\delta^2 u}{\delta^2 y}, u=u(y,t)$$

Magnetoelastic resonance is observed when the frequency of applied field matches the mechanical resonant frequency of the microribbon

$$f_o=\sqrt{\frac{E}{\rho\left(1-\sigma^2\right)}}\cdot\frac{1}{2l}$$

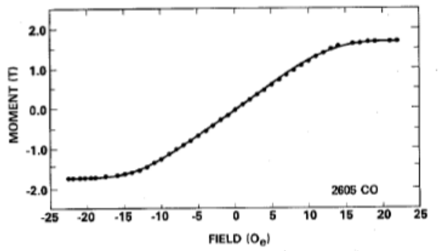

Fig. 2. Magnetization versus field for an annealed ribbon (T_a = 369°C, H_a = 6.1 k Oe). Scaling of the moment was accomplished by assuming that the sample is close to saturation with a saturation moment of 1.75T.

Amorphous ribbon

2826MB, Metglas, Conway, SC, USA

58 KHz

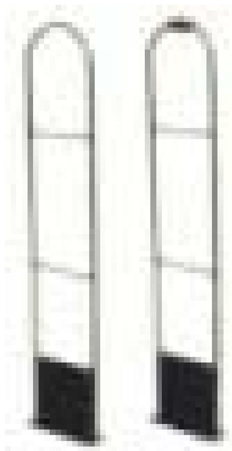

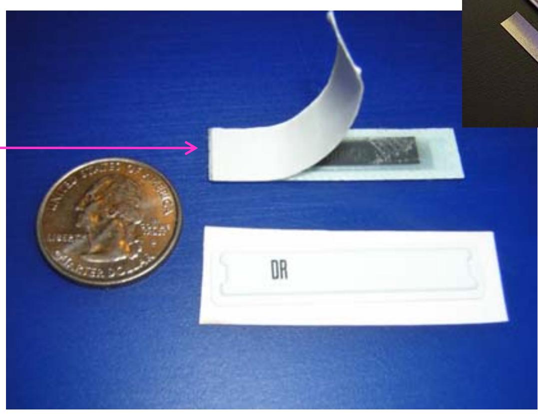

Acoustomagnetic tags

IEEE Sensors Council IEEE SENSORS JOURNAL, VOL. 23, NO. 2, 15 JANUARY 2023 1099

High-Sensitivity Wireless Sensing Using Amorphous Magnetic Microwires

B. T. Lejeune, Papa Gorgui Birame Gueye, Diego Archilla Sanz, Elena Navarro, Manuel Vazquez, *Senior Member, IEEE*, Rafael Perez del Real, *Member, IEEE*, Laura H. Lewis, and Pilar Marín

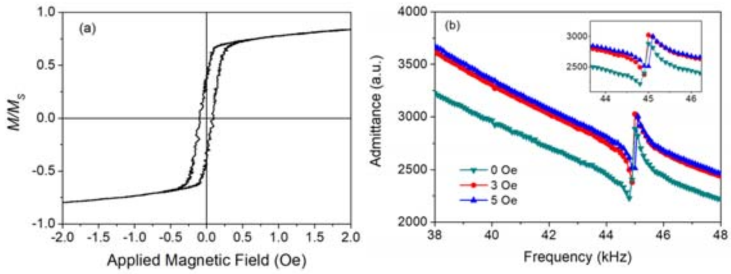

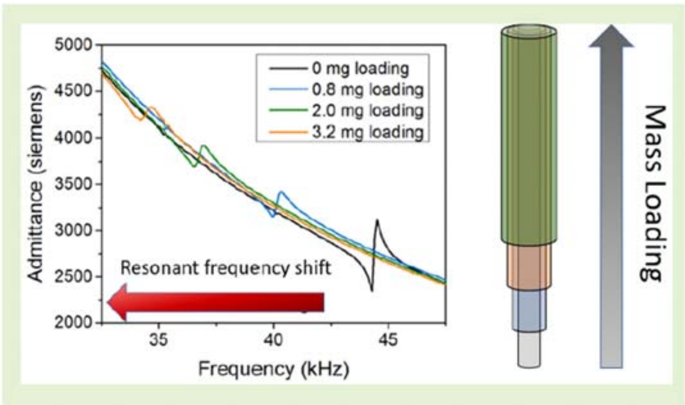

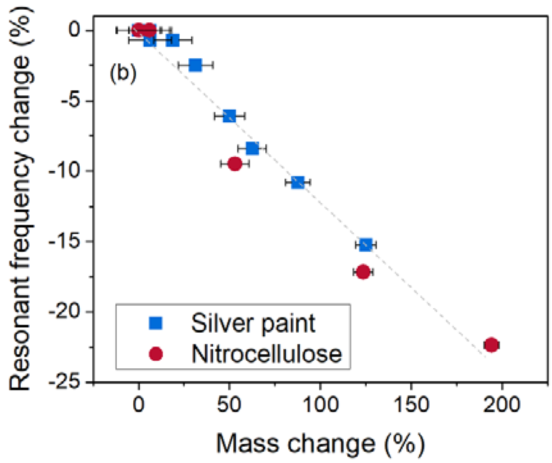

ima

biosensors

Real-Time Monitoring of Breath Biomarkers with a Magnetoelastic Contactless Gas Sensor: A Proof of Concept

Alvaro Peña [1,*], Juan Diego Aguilera [1], Daniel Matatagui [1,2,3,*], Patricia de la Presa [1,2], Carmen Horrillo [3], Antonio Hernando [1,4,5,6] and Pilar Marín [1,2]

[1] *Instituto de Magnetismo Aplicado (IMA), Universidad Complutense de Madrid – Administrador de Infraestructuras Ferroviarias (UCM-ADIF), 28230 Las Rozas, Spain;*
[2] *Departamento de Física de Materiales, Universidad Complutense de Madrid (UCM), Madrid 28040, Spain*
[3] *Grupo de Tecnología de Sensores Avanzados (SENSAVAN), Instituto de Tecnologías Físicas y de la Información (ITEFI), Consejo Superior de Investigaciones Científicas (CSIC), Madrid 28006, Spain*
[4] *Donostia International Physics Center, Donostia 20018, Spain*
[5] *Instituto Madrileño de Estudios Avanzados (IMDEA) Nanociencia , Madrid 28049, Spain*
[6] *Departamento de Ingeniería, Universidad de Nebrija, Madrid 28015, Spain*
Correspondence: alvapena@ucm.es (A.P.); d.matatagui@ucm.es (D.M.)

Supported by:
GOBIERNO DE ESPAÑA MINISTERIO DE CIENCIA E INNOVACIÓN
Fundación General CSIC

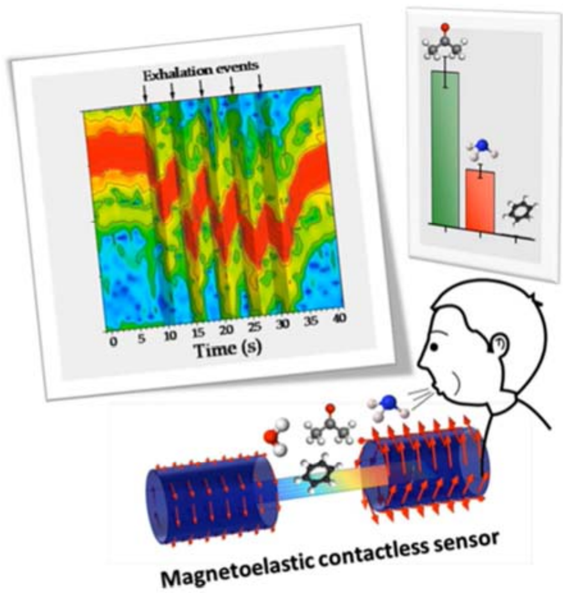

In this work, we have developted a real-time monitoring system of the resonant frequency on a magnetoelastic trasducer.

Acetone

Diabetes melitus

Ammonia

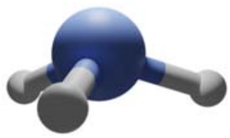

Hepatic and chronic kidney diseases (CKD), and cancers

Benzene

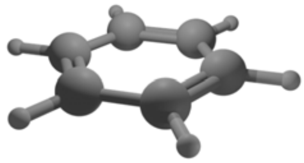

Sensor selectivity capacity

Schematics of the sensor cell, which includes cover (1), magnetoelastic microribbon (2), permanent magnet (3), and main body (4).

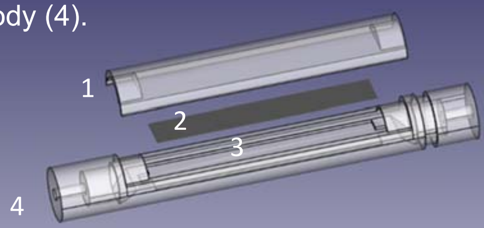

Figure 2. (**a**) Schematics of the oscillator circuit and electrical characterization setups for (**b**) frequency spectra and (**c**) real-time oscillator monitoring.

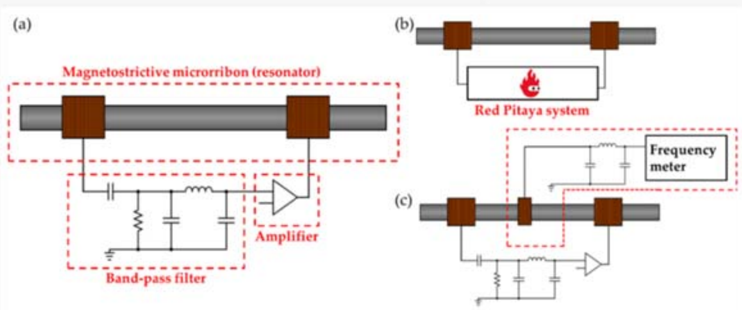

SEM images of the electrospun sensitive layer deposited over the transducer.

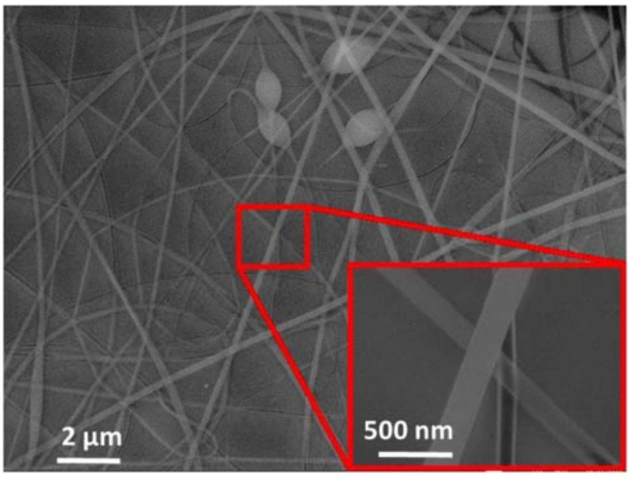

polyvinylpyrrolidone (PVP),

Frequency spectra of the transducer with and without the sensitive layer functionalization. Simulation results are used to illustrate the magnetoelastic resonance in the gain spectra for the no resonance state (NR) and the first (R1) and second (R2) harmonic of the magnetoelastic resonance.

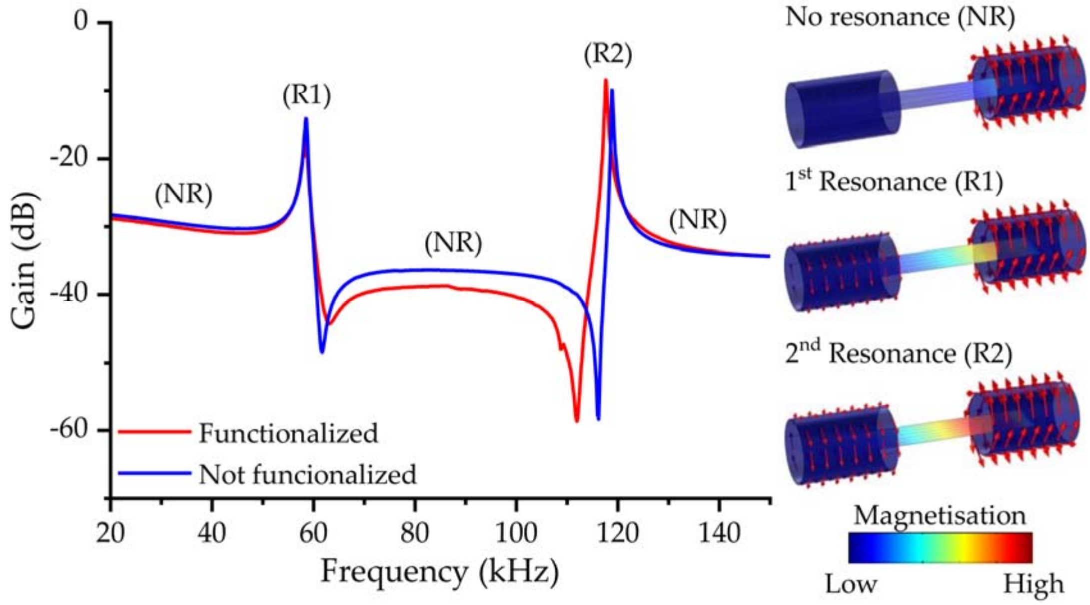

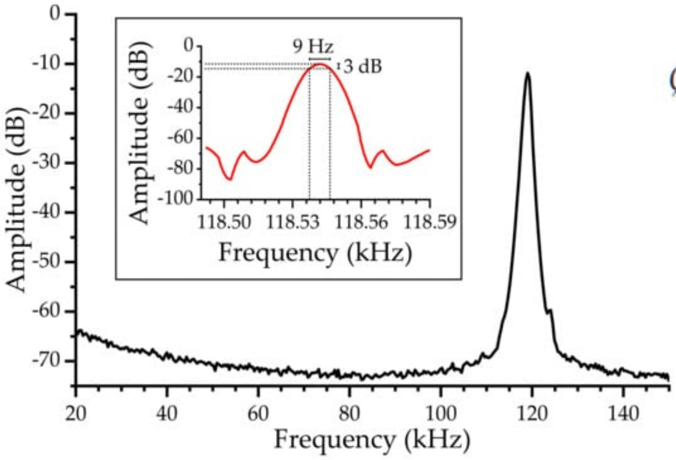

$$Q \stackrel{\text{def}}{=} 2\pi \times \frac{\text{energy stored}}{\text{energy dissipated per cycle}}$$

$$Q = \frac{f_c}{BW}$$

BW is the 3 dB bandwidth from the maximum amplitude

High-resolution frequency spectra for the quality factor determination with 13 Hz steps (black line) and 0.2 Hz steps (red line).

This work presents a proof of concept of the development of a magnetoelastic transducer and a measuring setup able to characterize resonant frequency in real time.

This transducer was functionalized with nanofibers of a sensitive polymer, polyvinylpyrrolidone (PVP),

to build a sensor capable of distinguishing between regular air and exhaled breath, as well as of quantitative and reproducible detection of relative humidity (RH), acetone, and ammonia in gaseous environments in a contactless, remote manner. In addition, benzene was used to test the sensor selectivity capacity.

Acetone

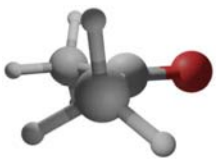

Diabetes melitus

Ammonia

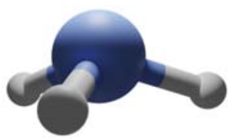

Hepatic and chronic kidney diseases (CKD), and cancers

Benzene

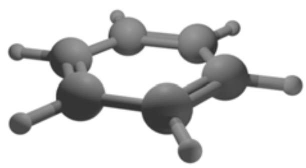

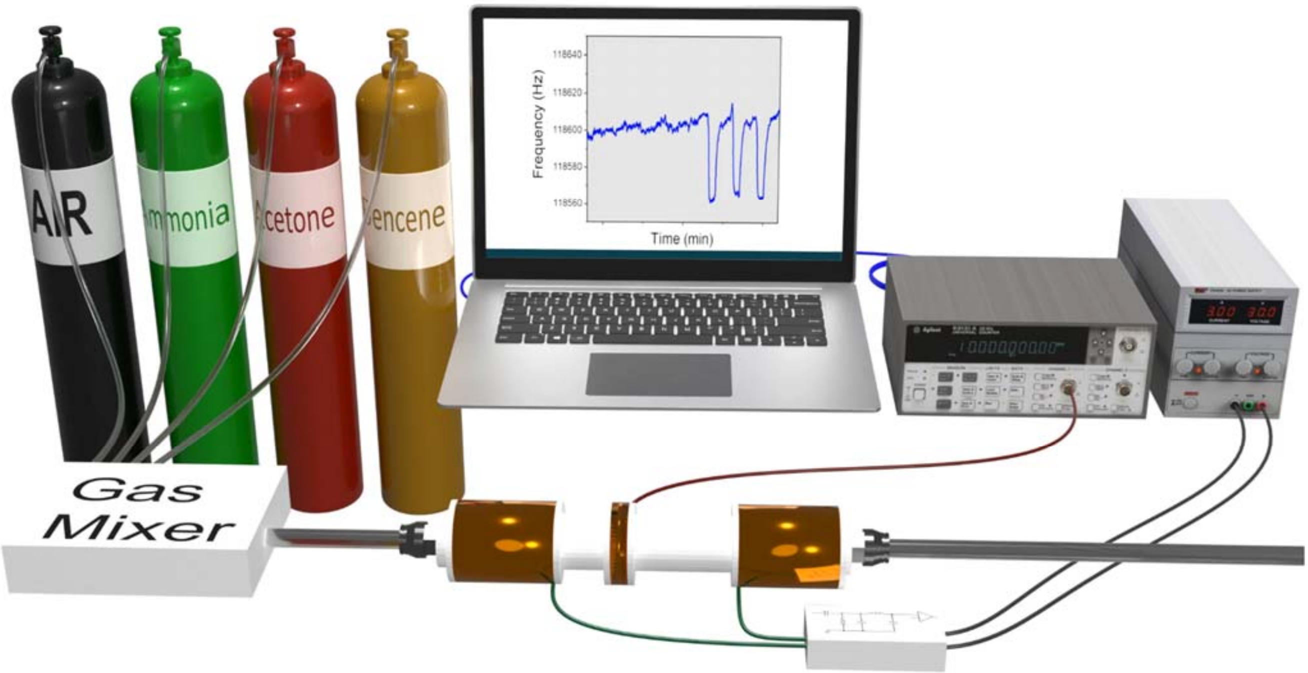

Relative Humidity tests

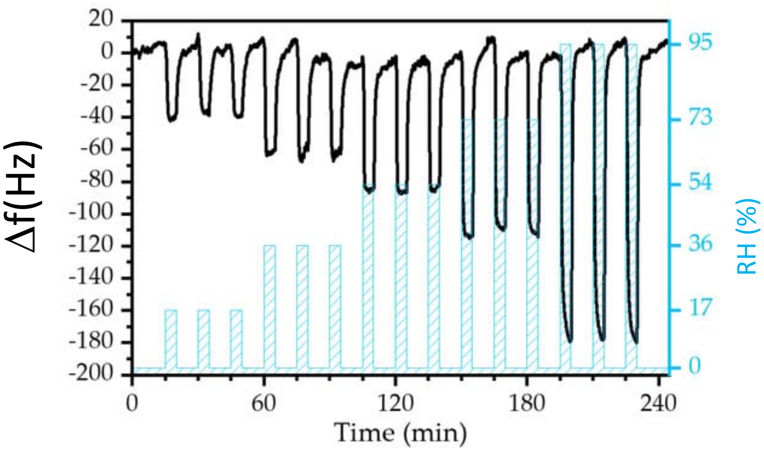

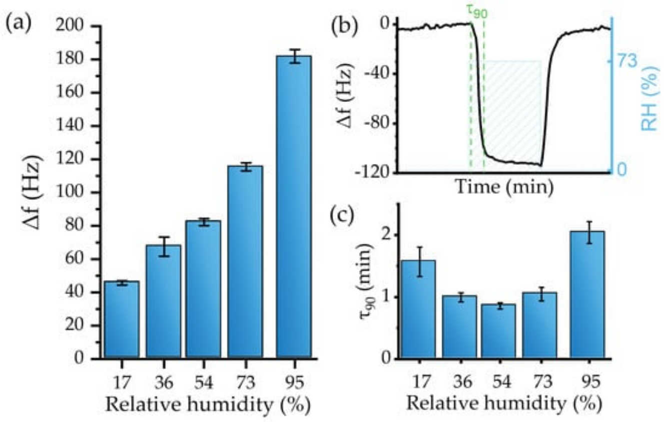

The sensitivity of the device, defined as the response to a specific concentration of the analyte (expressed in Hz/%), was obtained by fitting the values provided in Figure 9a. A linear response regime for levels up to RH = 73% was established. The linear fit provided a sensitivity of −1.17 ± 0.1 Hz/% (R^2 of 0.97).

The responsiveness time can be evaluated using the τ_{90} parameter, defined as the time required to achieve the 90% maximum frequency change (Figure 9b). In general, the sensor device showed a fast recovery with a low baseline drift for tested RH.

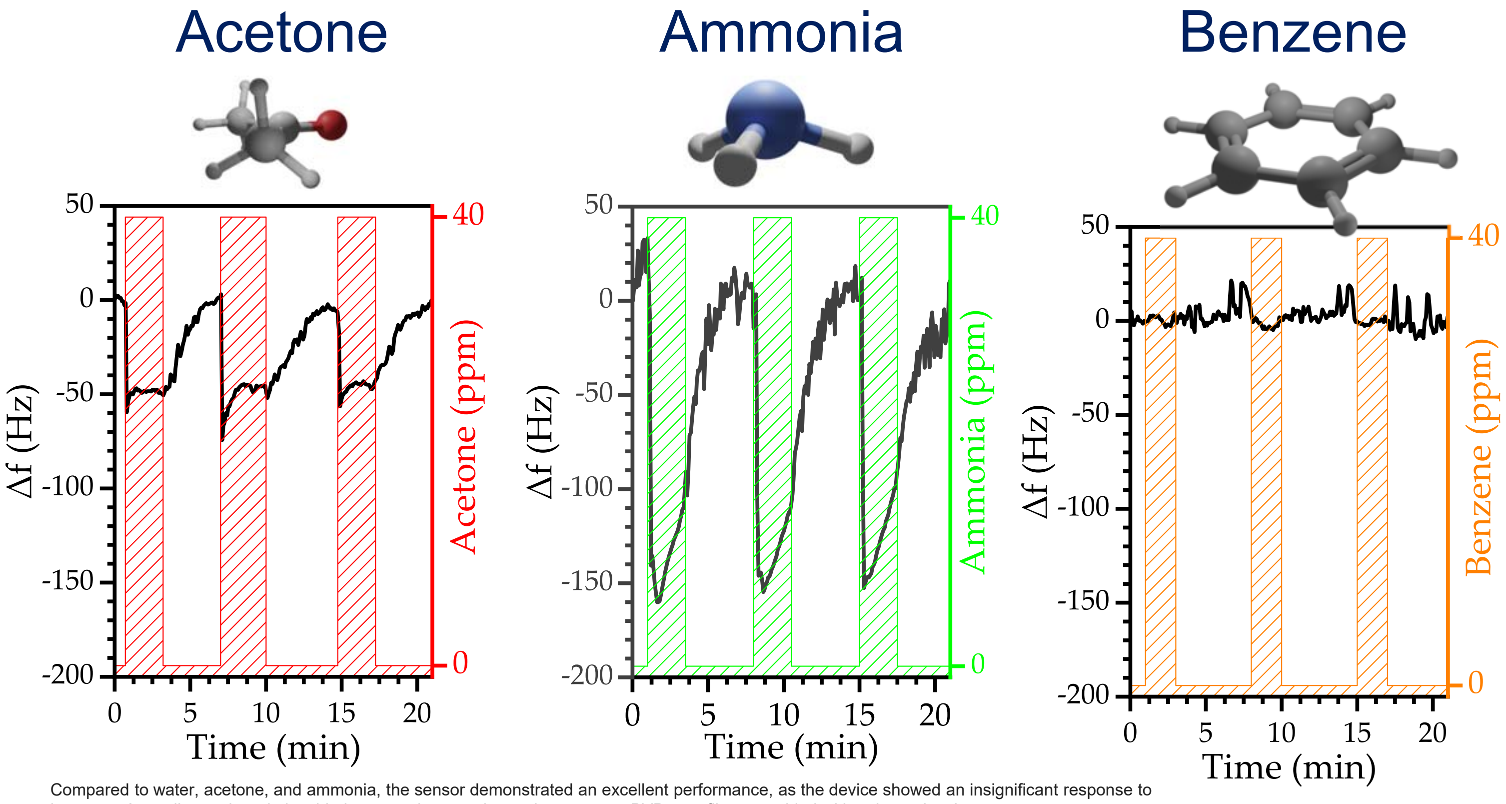

Compared to water, acetone, and ammonia, the sensor demonstrated an excellent performance, as the device showed an insignificant response to benzene. According to the relationship between the experimental responses, PVP nanofibers can bind with polar molecules, e.g., water, acetone, or ammonia with insignificant interaction with non-polar molecules such as benzene.

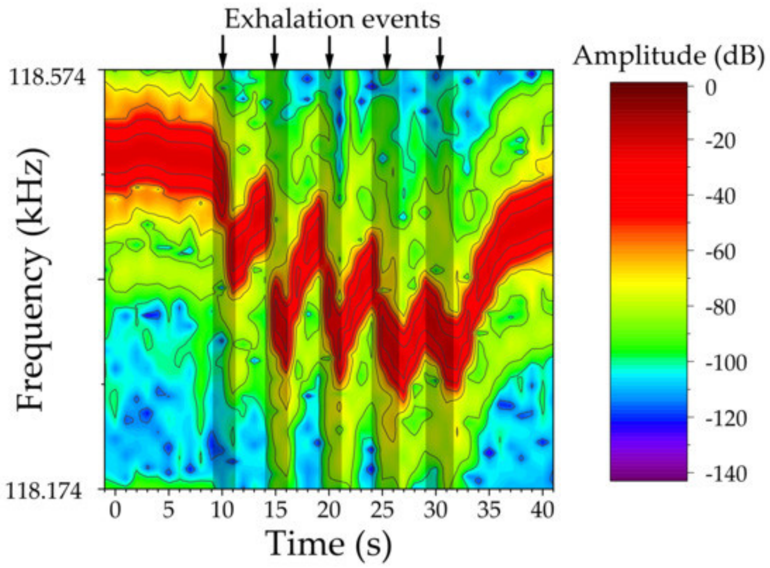


Sensing and Bio-Sensing Research 43 (2024) 100629

Contents lists available at ScienceDirect

Sensing and Bio-Sensing Research

journal homepage: www.elsevier.com/locate/sbsr

Real-time monitoring of breath biomarkers using magnonic wireless sensor based on magnetic nanoparticles

J.D. Aguilera[a], D. Arranz[a], A. Peña[a], P. Marín[a,b], M.C. Horrillo[c], P. de la Presa[a,b,*], D. Matatagui[a,b,*]

Magnonic-based magnetic transducer

Magnetostatic surface spin waves (MSSW)

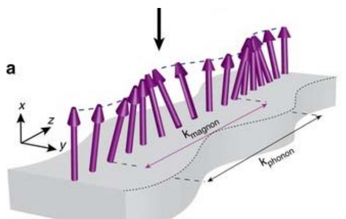

$$\omega = \sqrt{\frac{\omega_M^2}{2(coth(ks)+1)} + \omega_H^2 + \omega_M\omega_H}$$

$\omega_M = \gamma 4\pi M_s$ being M_S the

$\omega_H = \gamma H$ is the Larmor

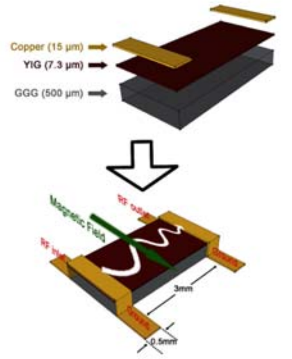

Figure 1. Schematic of a magnetostatic surface spin wave (MSSW) oscillator, which is the principal component of a magnonic gas sensor. The MSSW oscillator has a layered configuration (top), consisting of copper strips on top of yttrium ion garnet (YIG) and gadolinium gallium garnet (GGG) films. The magnetic field orientation of the device, which is used to obtain the MSSW propagation, is also shown (bottom). RF: Radio frequency.

Some important properties of MSSWs include their very low level of propagation loss at microwave frequencies, high-loaded 'Q value' (indication of under-damping), small wavelength, and high tunability (**from 0.2–20GHz**). We also note that the frequency of a spin-wave oscillator can be tuned by changing the magnitude of a bias magnetic field (HB), while the MSSW wavelength remains constant. In our case, we applied a bias magnetic field (about 200Oe) perpendicularly to the wave propagation direction and parallel to the YIG film plane

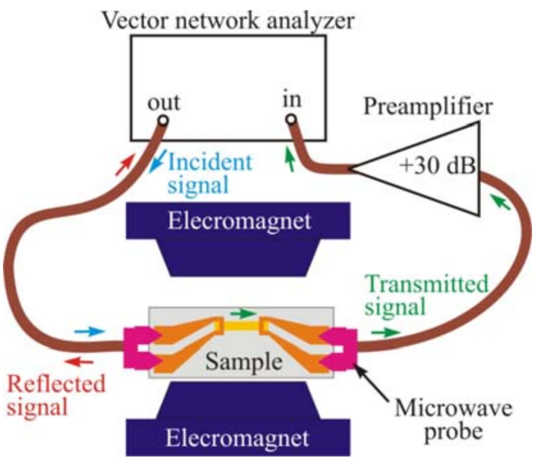

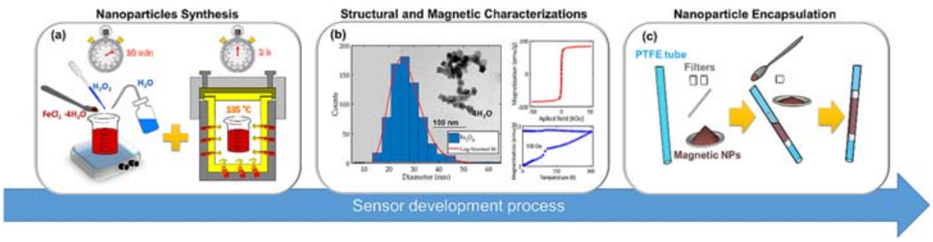

The synthesis of Fe_3O_4 was done by a hydrothermal method

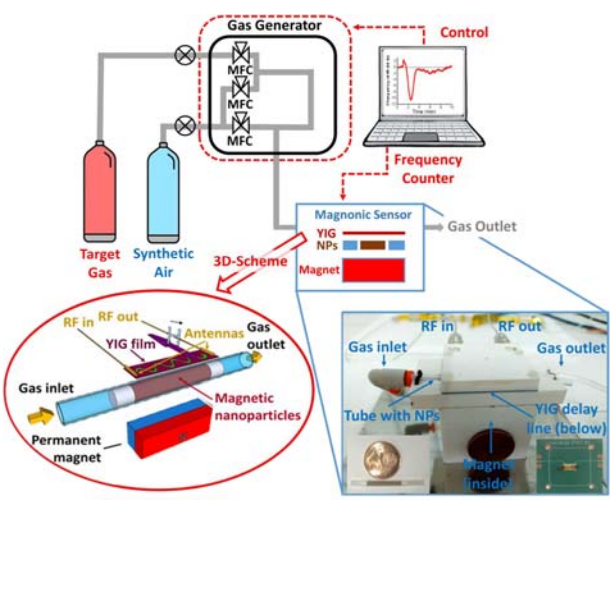

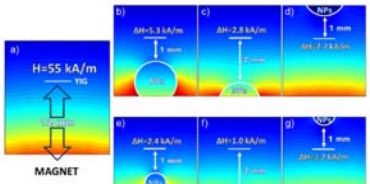

Fig. 3. Simulated variation of magnetic field H (ΔH) around the YIG film at different sizes and positions of the nanoparticles tube. (a) shows the field distribution over the cross section produced by the permanent magnet. From (b) to (d), 4 mm (diameter) nanoparticle tube is set just below the film (b), 2 mm further away (c) and just above the film (d). From (e) to (g), idem with 2 mm nanoparticle tube.

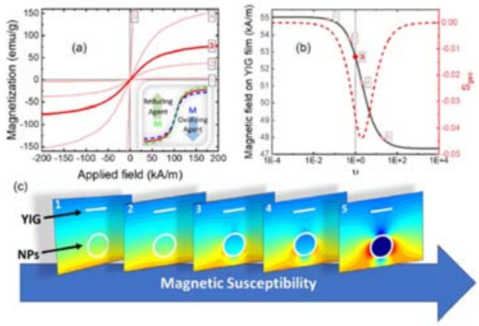

Fig. 4. Illustration of the process to calculate the magnetic sensitivity S_{mag}. The non-hysteretical magnetization curve M(H) (a) is vertically stretched or shrunk by multiplying magnetization by a factor ν (0.05, 0.5, 1, 2, 20) to obtain a family of curves $M_ν(H)$, and the image located in the lower-left corner illustrates how the magnetization of nanoparticles modulates when they interact with reducing and oxidizing gas agents. (b) The magnetic field on YIG film (black curve) and its derivative that represents the magnetic sensitivity (red curve). (c) Each curve is introduced into the Comsol model to obtain its associated $H_ν$. (For interpretation of the references to color in this figure legend, the reader is referred to the web version of this article.)

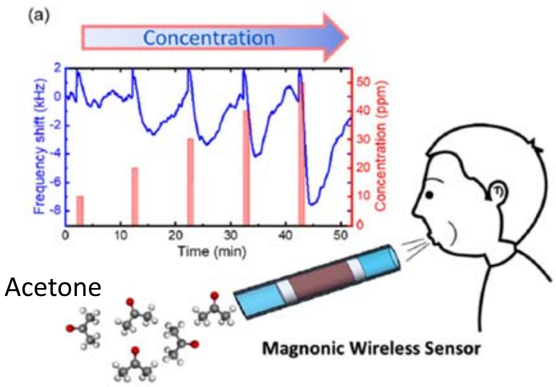

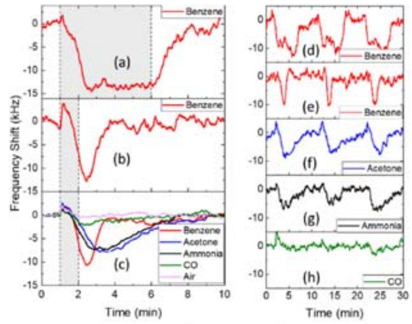

Fig. 5. (a) Response of the device to 50 ppm benzene with exposure times of 5 min. (b) Response of the device to 50 ppm benzene with exposure times of 1 min. (c) Mean response (10 measurements) of the device to the full cylinder concentration of the four gases and pure air. (d) Response of the device to three consecutive 5 min exposition events using benzene 50 ppm. (e-h) Response of the device to three consecutive exposition events using four target gases, with full cylinder concentrations (50 ppm (e-g), and 10 ppm (h)).

First, and as it is shown in the hysteresis loops presented in Fig. 4(a), Fe_3O_4 nanoparticles have high susceptibility.

Secondly, it has been reported an increase in the Fe^{2+}/Fe^{3+} cations ratio in Fe_3O_4 nanoparticles under the presence of gaseous benzene, toluene, ethylbenzene, and o-xylene (BTEX) at room temperature and atmospheric pressure [39], indicating a relative good physisorption of these gases. And even though to the best of our knowledge there is no literature about the physisorption of acetone, ammonia, or carbon dioxide by Fe_3O_4 nanoparticles, a similar mechanism could be expected due to their reducing nature. The change in the Fe^{2+}/Fe^{3+} ratio can induce significant changes in the magnetic behaviour of the surface atoms [40] and, given the high surface to volume ratio, this change can

It is noteworthy that the sensor exhibits the capability to successfully detect acetone (diabetes mellitus biomarker) at concentrations between 20 and 50 ppm within a brief exposure time of 1 min. This achievement was accompanied by remarkable recovery and reproducibility rates, as well as distinct response parameters compared among biomarkers.